11th International Conference on Vibration Problems
Z. Dimitrovová *et.al.* (eds.)
Lisbon, Portugal, 9–12 September 2013

NUMERICAL SIMULATION OF THE DYNAMIC BEHAVIOUR OF TURBOCHARGERS UNDER CONSIDERATION OF FULL-FLOATING-RING BEARINGS AND BALL BEARINGS

Christian Daniel[1], **Stefan Göbel**[1], **Steffen Nitzschke**[1],
Elmar Woschke*[1], **Jens Strackeljan**[1]

[1]Otto-von-Guericke-University - Institute of Mechanics (Technical Dynamics), Magdeburg, Germany
{christian.daniel, stefan.goebel, steffen.nitzschke, elmar.woschke, jens.strackeljan}@ovgu.de

Keywords: Run-up Simulation, Turbocharger, Full-floating-ring Bearing, Ball Bearing, Time Integration, Multibody Simulation.

Abstract. *This paper deals with the simulation of turbochargers run-up behaviour, whereat the focus is on the realistic description of the bearing unit. Along with full-floating-ring bearings, ball bearings and ball bearings with squeeze film dampers are applied. The rotordynamic simulation of the turbocharger is done within a multibody system, due to the nonlinear behaviour and the thereby associated requirements on the solver algorithm. The description of a full-floating-ring bearing is based on a transient numerical solution of Reynolds' equation at each step of time integration. The coupling of the lubrication films by communication drill holes as well as oil supply is considered by hydrodynamic boundary conditions. Depending on the kinematic quantities a pressure distribution is calculated, which is applied on the rotor. The implementation of the ball bearings includes the description of all bearing elements (inner ring, rolling bodies, bearing cage and outer ring) and their mutual interaction. Questions concerning contact detection, determination of normal and tangential forces together with the calculation of the resulting forces and moments are discussed. The bearing elements are formally modeled as rigid bodies, the computation of the contact forces is based upon formulation of Hertz. This provides a feasibility to consider resulting contour deformations in addition. Different run-up simulations of a defined test model with varying implementation of bearings are presented. Considerations relating to the nonlinear behaviour of the bearing variants are accomplished, which focus on the level of unbalance vibrations, instabilities like oil-whirl, and the behaviour at speeds close to resonance.*

1 INTRODUCTION

Turbochargers are essential elements in the downsizing concept of recent combustion engines. While their operation principle is quite easy, hot exhaust gases propel a turbine wheel which drives a compressor wheel via a conjoint shaft, it is challenging to predict the operation behavior. One major development objective is to raise the maximum rotor speed to either increase the air-mass flow or decrease design size. This causes, among mechanical strength issues, inadequate subsynchronous vibrations and instability phenomenons known as fluid-whirl and fluid-whip for chargers equipped with journal bearings [1, 2]. A second objective is to reduce friction loss, especially during cold start situations. Therefore ball bearings are most suitable. The first part of this paper is about how different kinds of bearings can be modeled as nonlinear force elements within a multibody simulation. The reader must be aware of the fact, that for a run-up of 4 seconds, like simulated for this paper, about 10 million calls of the force elements are necessary. From this it follows that a single call must be calculated by fractions of a second. A high time efficiency is reached by integrated computation of rigid body motion, elastic deformation and bearing forces within one program. Differences in view of dynamic behaviour and bearing forces between a turbocharger mounted in three various bearing variants are presented and discussed in the second part of the paper.

2 MECHANICAL MODEL OF THE TURBOCHARGER

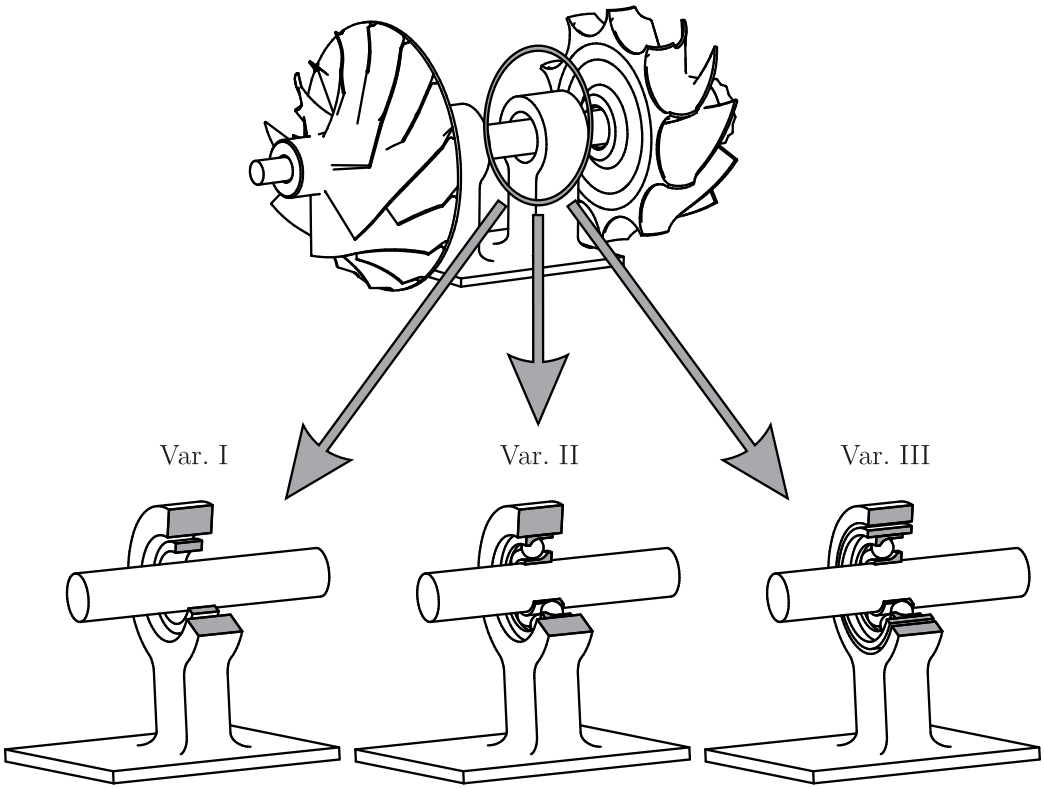

Figure 1: Model of the turbocharger with different bearing types.

A schematic representation of the turbocharger is given in Figure 1. The rotor consists of the two rigid bodies turbine and compressor wheel, which are both fixed on a bending elastic

shaft. This shaft is modeled by an unreduced Timoshenko-beam finite element formulation (see Chapter 2.1.1) . For the presented examination the rotor is supported by three different bearing types. Variant I means a full-floating ring bearing whereat the rings are two rigid bodies within the simulation. Variant II means ball bearings with inner as well as outer ring, 8 balls and a cage summed up to 11 additional bodies. Variant III means a support in ball bearings like Varariant II, but themselves placed within a squeeze film damper towards the pedestal. Due to the multibody representation of all bearing parts the mass and inertia forces are, in contrast to an iterative static proceeding, inherently contained. Restoring forces of the bearings are part of the right-hand side in the differential equations of motion. The presented simulations are carried out for a run-up to 150,000 rpm in 4 s. Some significant model data can be found in Table 1. The investigated charger is at the typical size for a light duty commercial vehicle.

Body	Parameters	Values	
rotor	length	≈ 140	mm
	shaft diameter	10	mm
	rotor mass	≈ 0.450	kg
	unbalance turbine wheel	580	$mgmm$
	unbalance compressor wheel	390	$mgmm$
floating ring bearing	inner diameter/width	$10/7$	mm
	outer diameter/width	$16/10$	mm
	oil viscosity grade	$20W30$	
	supply pressure	4.5	bar
	supply temperature/ pressure	90	$°C$
ball bearing	number of balls	8	
	ball diameter	4.5	mm
squeeze film damper	diameter/width	$20.5/6$	mm
	clearance	0.005	$[-]$
	oil viscosity grade	$20W30$	
	supply pressure	4.0	bar
	supply temperature/ pressure	90	$°C$

Table 1: Selected model data.

2.1 Equations of motion

2.1.1 Elastic deformation of the shaft

The elastic properties of the rotor assembly are widely determined by the shaft, hence both wheels can be assumed as rigid bodies. The assembly performs small motions, except the rotation around the longitudinal axis. Therefore the overall-motion can be described by means of a linear finite element model. As the main dimension of the shaft is determined by its length, taking into account the existence of short shoulders, a beam model based on the Timoshenko-theory is assumed. To derive the equations of motion the principle of virtual work is used

$$\delta W_e = \delta W_o - \delta W_i \quad . \tag{1}$$

The elastic part of virtual work can be identified as

$$\delta W_e = \int_V \delta(u' - \psi_y) GA_s \left(u' - \psi_y\right) + \delta(v' - \psi_x) GA_s \left(v' - \psi_x\right) dm + \int_V \delta\psi_x' EI_{xx} \psi_x' + \delta\psi_y' EI_{yy} \psi_y' \, dm \quad , \tag{2}$$

in which GA_s and EI are referring to shear- and bending-stiffness. The virtual work due to outer loads F_i, M_i and the line loads q_i results in

$$\delta W_o = \int_V \delta u \, q_x + \delta v \, q_y \, dm + \delta u F_x + \delta v F_y + \delta\psi_x M_x + \delta\psi_y M_y \quad . \tag{3}$$

The last term in Eq. 1 represents the inertia loads including the effects due to rotation of the shaft. For its determination it is necessary to develop the position vector $\vec{r}$,which points to the infinitesimal mass element dm, in coordinates of the body fixed reference frame K and the corresponding absolute acceleration $\ddot{\vec{r}}$ (see Figure 2). Both absolute acceleration and virtual displacement δr must be derived in the inertial system I, using the transformation $\underline{\underline{A}}_{IK}$.

$$\delta W_i = \int_V \delta\vec{r}\,\ddot{\vec{r}}\, dm = \int_V {}_I\delta r \, {}_I\ddot{r} \, dm \quad , \tag{4}$$

$${}_I\underline{r} = \underline{\underline{A}}_{IK} \left({}_K(\underline{r}_Z + \underline{r}_E) + \underline{\underline{A}}_{KE} \, {}_E\underline{r}_P \right) \quad , \tag{5}$$

$${}_I\delta\underline{r} = \underline{\underline{A}}_{IK} \left({}_K\delta\underline{r}_E + \delta\underline{\underline{A}}_{KE} \, {}_E\underline{r}_P \right) \quad , \tag{6}$$

$$\begin{aligned} {}_I\ddot{\underline{r}} = {} & \ddot{\underline{\underline{A}}}_{IK} \, {}_K(\underline{r}_Z + \underline{r}_E) + 2\,\dot{\underline{\underline{A}}}_{IK} \, {}_K\dot{\underline{r}}_E + \underline{\underline{A}}_{IK} \, {}_K\ddot{\underline{r}}_E \\ & + \ddot{\underline{\underline{A}}}_{IK} \underline{\underline{A}}_{KE} \, {}_E\underline{r}_P + 2\,\dot{\underline{\underline{A}}}_{IK} \dot{\underline{\underline{A}}}_{KE} \, {}_E\underline{r}_P + \underline{\underline{A}}_{IK} \ddot{\underline{\underline{A}}}_{KE} \, {}_E\underline{r}_P \quad . \end{aligned} \tag{7}$$

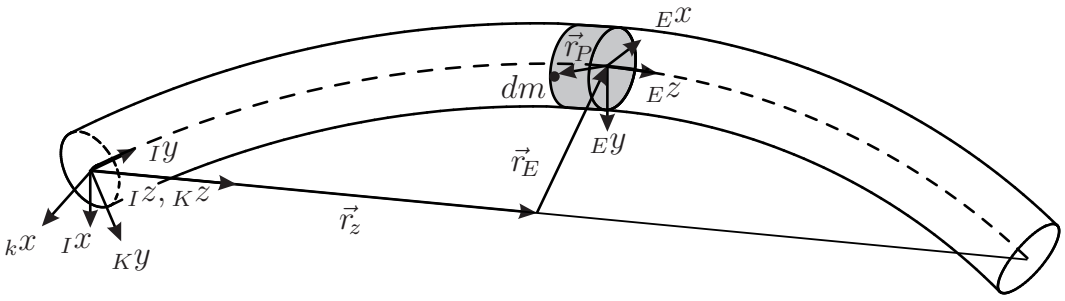

Figure 2: Position vector to mass element dm.

The meaning of the in Eqs. (4-7) used vectors can be taken from Figure 2, however ${}_K\underline{r}_E$ contains the translational degrees of freedom (u, v), whereat the rotational ones (ψ_x, ψ_y) form the transformation matrix $\underline{\underline{A}}_{KE}$. To achieve a finite element formulation of Eq. 1 the usual approaches are introduced

$$\begin{aligned} u(z,t) &= \underline{N}_V^T(z)\,\underline{u}(t) & \psi_y(z,t) &= \underline{N}_W^T(z)\,\underline{u}(t) & & \\ v(z,t) &= \underline{N}_V^T(z)\,\underline{v}(t) & \psi_x(z,t) &= \underline{N}_W^T(z)\,\underline{v}(t) & & \text{with} \\ \underline{N}_V^T(z) &= [f_1\ f_2\ f_3\ f_4] & \underline{N}_W^T(z) &= [f_5\ f_6\ f_7\ f_8] & & \text{and} \\ \underline{u}(t) &= [u_1\ \psi_{y1}\ u_2\ \psi_{y2}] & \underline{v}(t) &= [v_1\ \psi_{x1}\ v_2\ \psi_{x2}] & . & \end{aligned} \tag{8}$$

The shape functions f_i can be found by analytical solution of static Timoshenko-beam equations with unity boundary conditions and turn out to be cubical polynomials for $f_{1...4}$ and quadratic for $f_{5...8}$ respectively. Applying these approaches into Eq. 1 considering the linear terms leads to finite element equations of motion for the shaft

$$\underline{\underline{M}}\,\ddot{\underline{x}} + \left(\underline{\underline{D}} + \Omega\,\underline{\underline{G}}\right)\dot{\underline{x}} + \left(\Omega^2\,\underline{\underline{M}}_\Omega + \underline{\underline{K}}\right)\underline{x} = \underline{f} \quad . \tag{9}$$

2.1.2 Rigid bodies

In the carried out simulation rigid bodies are mainly used to describe the interaction of ball bearing elements. Whereat in Chapter 2.1.1 linear equations could be derived, as a result of large displacements a non-linear description is necessary here. Therefore a multibody algorithm [3], derived by the equilibrium of forces and moments with respect to the body fixed reference frame K in point A, is applied

$${}_K\underline{\underline{M}}\,{}_K\underline{a} + {}_K\underline{h}_\omega = {}_K\underline{h}_e \quad , \tag{10}$$

which is suitable to calculate the actual acceleration ${}_K\underline{a}$ according to external forces ${}_K\underline{h}_e$ as well as to centrifugal and coriolis forces ${}_K\underline{h}_\omega$. The vector ${}_K\underline{a}$ includes the translational and rotational acceleration

$${}_K\underline{a} = ({}_K\underline{v}'_A \quad {}_K\dot{\underline{\omega}})^T, \tag{11}$$

the constant symmetric mass matrix consists of the mass m, the center of gravity ${}_K\underline{c}_S$ as well as the moment of inertia tensor ${}_K\underline{\underline{J}}^A$

$${}_K\underline{\underline{M}} = \begin{bmatrix} m\,\underline{\underline{E}} & -m\,{}_K\underline{\underline{\widetilde{c}}}_S \\ m\,{}_K\underline{\underline{\widetilde{c}}}_S & {}_K\underline{\underline{J}}^A \end{bmatrix} \quad , \tag{12}$$

the centrifugal and coriolis forces can be written as

$${}_K\underline{h}_\omega = \begin{pmatrix} m\,{}_K\underline{\omega} \times {}_K\underline{v}_A & + & m\,{}_K\underline{\omega} \times ({}_K\underline{\omega} \times {}_K\underline{c}_S) \\ {}_K\underline{\underline{\widetilde{\omega}}}\,{}_K\underline{\underline{J}}^A\,{}_K\underline{\underline{\widetilde{\omega}}} & + & m\,{}_K\underline{c}_S \times ({}_K\underline{\omega} \times {}_K\underline{v}_A) \end{pmatrix} \tag{13}$$

and the external forces and torques are given by

$${}_K\underline{h}_e = \begin{pmatrix} {}_K\underline{F}_e \\ {}_K\underline{M}_e^A \end{pmatrix}. \tag{14}$$

To solve Eq. 10 a state-space description is essential, defining the state-space as

$$\underline{z} = [{}_K\underline{r}_A \quad \underline{x} \quad {}_K\dot{\underline{r}}_A \quad {}_K\underline{\omega}]^T \quad \text{with} \quad \underline{x}^T = [\alpha \;\; \beta \;\; \gamma]^T \quad , \tag{15}$$

whereas the spatial arrangement is represented by gimbal angles merged in the vector $\underline{x}$. The time derivation of $\underline{x}$ has to be determined by the angular velocity ${}_K\underline{\omega}$

$$\dot{\underline{x}} = {}_K\underline{\underline{H}}_R^{\;-1}\,{}_K\underline{\omega} = \begin{bmatrix} \dfrac{cos(\gamma)}{cos(\beta)} & -\dfrac{sin(\gamma)}{cos(\beta)} & 0 \\ sin(\gamma) & cos(\gamma) & 0 \\ -cos(\gamma)\,tan(\beta) & sin(\gamma)\,tan(\beta) & 1 \end{bmatrix} {}_K\underline{\omega} \quad . \tag{16}$$

Finally the so transformed Eq. 10 can be solved with arbitrary ode-solvers.

2.2 Ball bearings

The motion of each bearing part can be calculated by use of the equations from Chapter 2.1.2. Furthermore the interactions of these bodies has to be taken into account, which basically represents a contact problem, resulting in the necessity to calculate the normal and tangential force at each contact point. Due to the high number of potential contact points and to ensure a fast and reliable calculation of contact forces an analytical contact algorithm has been chosen.

Determination of contact At first the normal distance δ_K between the potential contact points K_1 and K_2 , described by ${}_I\underline{r}_{K1}$ and ${}_I\underline{r}_{K2}$, has to be calculated (see Figure 3). The contact status changes with sign of δ_K, whereat $\delta_K < 0$ identifies closed contact. The two-dimensional contact between to rigid bodies with a circular contour can be calculated analytically, using relative kinematics. The potentially contact points K_1 and K_2 can be calculated with the known position of each body's centre point

$$ {}_I\underline{r}_{K1} = {}_I\underline{r}_{A1} + {}_I\underline{s}_1 \quad , \qquad {}_I\underline{r}_{K2} = {}_I\underline{r}_{A2} + {}_I\underline{s}_2 \quad . \tag{17} $$

The position vector between the centre points ${}_I\underline{L}_M$ is used to calculate the local position vector from the centre point to the outline of the body

$$ {}_I\underline{L}_M = {}_I\underline{r}_{A2} - {}_I\underline{r}_{A1} \quad , \tag{18} $$

$$ {}_I\underline{s}_1 = \frac{{}_I\underline{L}_M}{|{}_I\underline{L}_M|} R_1 \quad , \qquad {}_I\underline{s}_2 = -\frac{{}_I\underline{L}_M}{|{}_I\underline{L}_M|} R_2 \quad . \tag{19} $$

The normal vector of the surface in the contact points can be calculated from $\underline{s}_1$ and $\underline{s}_2$

$$ {}_I\underline{n}_1 = \frac{{}_I\underline{s}_1}{|{}_I\underline{s}_1|} \quad , \qquad {}_I\underline{n}_2 = -\frac{{}_I\underline{s}_2}{|{}_I\underline{s}_2|} \quad , $$

leading to the normal penetration

$$ \delta_K = ({}_I\underline{r}_{K2} - {}_I\underline{r}_{K1})\, {}_I\underline{n}_1 \quad . $$

The penetration velocity $\dot{\delta}_K$ can be determined by usage of the velocities $\underline{v}_{K1}$ and $\underline{v}_{K2}$

$$ \dot{\delta}_K = ({}_I\underline{v}_{K2} - {}_I\underline{v}_{K1})\, {}_I\underline{n}_1 \quad . $$

Calculation of the normal contact forces The relation between contact force and elastic deformation of two bodies with a spherical contour was described by Hertz [4]. The resulting formulae are suitable to calculate the size of the contact area with respect to the normal contact force. For the present application the inverse function Eq. 20 is needed, which yields the normal contact force F_{HP} according to the actual penetration δ_K

$$ F_{HP}(\delta_K) = -\sqrt{\frac{E'^2\, 3}{\rho'} \left(\frac{2\,|\delta_K|}{3\,\mu^*}\right)^3} \quad , \tag{20} $$

$$ \rho' = \frac{1}{R_{x1}} + \frac{1}{R_{y1}} + \frac{1}{R_{x2}} + \frac{1}{R_{y2}} \quad , $$

$$ \frac{1}{E'} = \frac{1}{2}\left(\frac{1-\nu_1^2}{E_1} + \frac{1-\nu_2^2}{E_2}\right) \quad , $$

$$ \mu^* = 0.171 \text{ (for cylinder against sphere)} \quad . $$

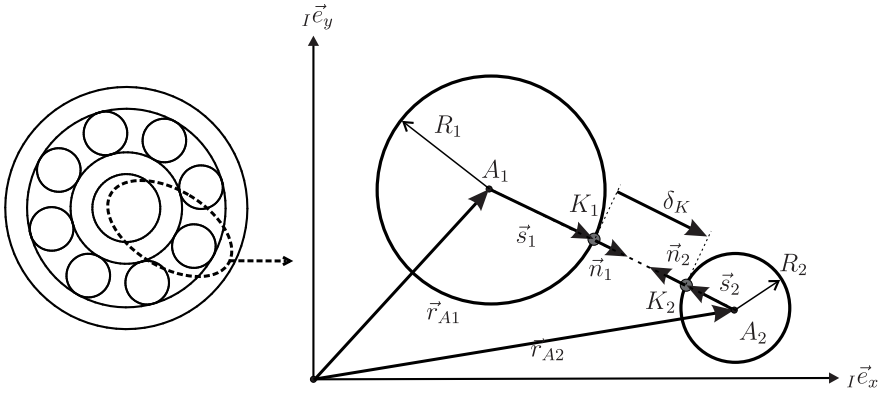

Figure 3: Contact-detection between spheres.

The dissipative part is formulated by a linear damping constant d. The resulting normal contact force consists of the hertzian and the dissipative part, depending on contact status

$$F_N = \begin{cases} F_{HP}(\delta_K) + \dot{\delta}_K\, d & \text{if } \delta_K \leq 0 \\ 0 & \text{if } \delta_K > 0 \end{cases} \quad . \tag{21}$$

Calculation of the tangential contact forces The tangential contact force is modeled with a coulomb approximation

$$F_T = F_N\, \mu(v_t) = F_N\, \mu_r\, \operatorname{sgn}(v_t) \quad . \tag{22}$$

To improve the results for this discontinuous function the friction coefficient is assumed to be a function of the relative tangential velocity v_t

$$\mu(v_t) = \left(\mu_r + (\mu_0 - \mu_r)\, \mathrm{e}^{-\frac{v_t}{v_1}\, \operatorname{sgn}(v_t)}\right) \tanh\left(\frac{v_t}{v_2}\right) \quad . \tag{23}$$

The transition between adhesion and friction is realised by an additional term with an exponential scaling of the relativ velocity. Thus for relative velocities in the range of v_1 the friction coefficient μ is nearly μ_0. If the relative velocity is greater than v_2 the coefficient will converge to μ_r .

2.3 Journal and full-floating ring bearings

The hydrodynamic pressure generation in a full-floating-ring bearing is described by the Reynolds' partial differential equation (R-PDE) for both, the inner and the outer lubrication film

$$\frac{\partial}{\partial x}\left(\frac{h^3}{\eta}\frac{\partial p}{\partial x}\right) + \frac{\partial}{\partial z}\left(\frac{h^3}{\eta}\frac{\partial p}{\partial z}\right) = 6(U_1 + U_2)\frac{\partial h}{\partial x} + 12\frac{\partial h}{\partial t} \quad . \tag{24}$$

An analytical solution of this PDE is not existent, hence Eq. 24 has to be discretized under usage of the finite difference method (FDM) or finite element method (FEM) and solved numerically as described in [5]. Caused by the high clearance of the outer bearing the rotating assembly is able to take a skew position, which results in a non-parallel gap for the inner bearing. This leads mainly to an additional damping moment.

The implementation of the boundary conditions is of importance. Beside the Dirichlet- and the periodical boundary conditions the coupling of both lubrication films via the communication drill-holes has to be taken into account. To avoid interpolations, this leads to a description of both lubrication films with the floating ring as reference system [5, 6, 7]. Further the fresh oil supply at the outer lubrication film has to be modelled in an adequate way. Supplemental points concerning the implementation of cavitation effects, microhydrodynmics and turbulence are neglected in this paper.

3 NUMERICAL RESULTS

The results of the numerical computations of the different in Chapter 2 introduced bearing variants are compared in this section concerning the displacements of the shaft as well as the bearing forces at the compressor side. Illustrations are achieved by spectrograms showing the containing frequencies f at each rotational frequency f_d of the rotor during the run-up.

3.1 Journal bearings

In the displacement plot Figure 4 (left) a straight frequency branch can easily be identified as synchronous and unbalance induced. Furthermore subsynchronous frequencies can be seen. They are characteristic for low loaded fluid bearings and well described as self-excited whirl phenomenon [2]. In a nutshell the circumferental oil at the velocity of any around half the shaft speed excites the rotor. As already mentioned the bearing is a floating ring one, that means it is divided into two fluid films.

The explanation of the first subsynchronous branch starting from $100\,Hz$ is a whirl in the inner oil film. Its frequency increases slightly with the rotor speed. At $f_d \approx 600\,Hz$ the vibration frequency suddenly changes to $400\,Hz$. This jump effect is due to the achievement of the second rotor eigenfrequency according to [8]. After this vibration decayed a second group of subsynchronous frequencies appear at $f_d \approx 1300\,Hz$. The lower one is a whirl in the outer oil film, the higher one is a side band as it is typical for nonlinear force elements. In the force plot on the right side even a second side band can be identified.

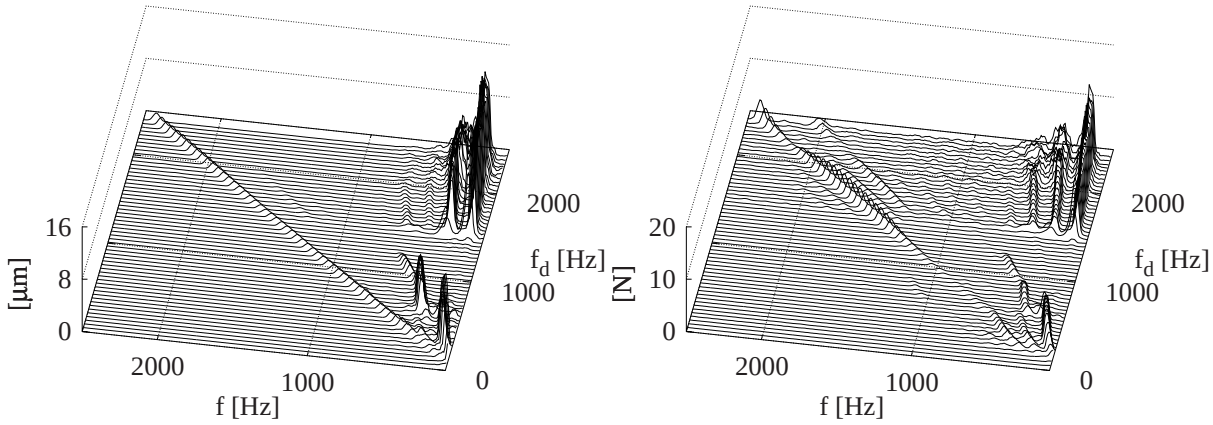

Figure 4: Support in journal bearings: displacement of the compressor wheel (left), bearing force(right) .

Comparison of amplitudes shows much smaller displacements caused by unbalance response as due to oil-whirl vibration. Note the maximum displacement of about $15\,\mu m$ and maximum bearing force of $17\,N$.

3.2 Ball bearings

The second variant to support the turbocharger shaft are ball bearings. One advantage compared to the fluid-bearings is the elimination of any subharmonic vibrations. The stiffness is nearly constant, and the oil supply can be designed easier. The disadvantages are small damping ratios and the need to pre-load the bearings to ensure a confident roll-off of the balls within the bearing. Due to this fact spindle ball bearings have to be used for light-loaded applications, which are much more costly compared to fluid bearings.

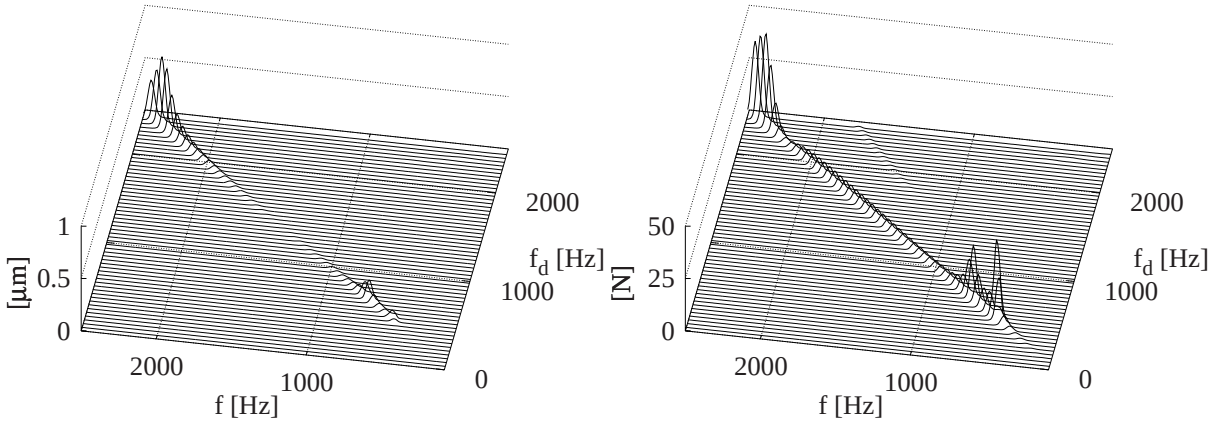

Figure 5: Support in roller bearings: displacement of the compressor wheel (left), bearing force(right) .

Figure 5 (left) shows again the spectrogram of shaft vibration. As expected there exist only synchronous vibrations caused by the unbalance of compressor and turbine wheels. The spectrogram of force on the right side illustrates one magnification during pass of the first and second resonance at $500\,Hz$ and $700\,Hz$ and one during the third resonance at $2300\,Hz$. The level of vibration in the resonance reflects the low damping ratio of ball bearings. The maximum displacements of the compressor wheel amount to less than $1\,\mu m$ and are much smaller than with fluid bearings, in contrast the force amplitude raises to $48\,N$.

3.3 Ball bearings with squeeze film damper

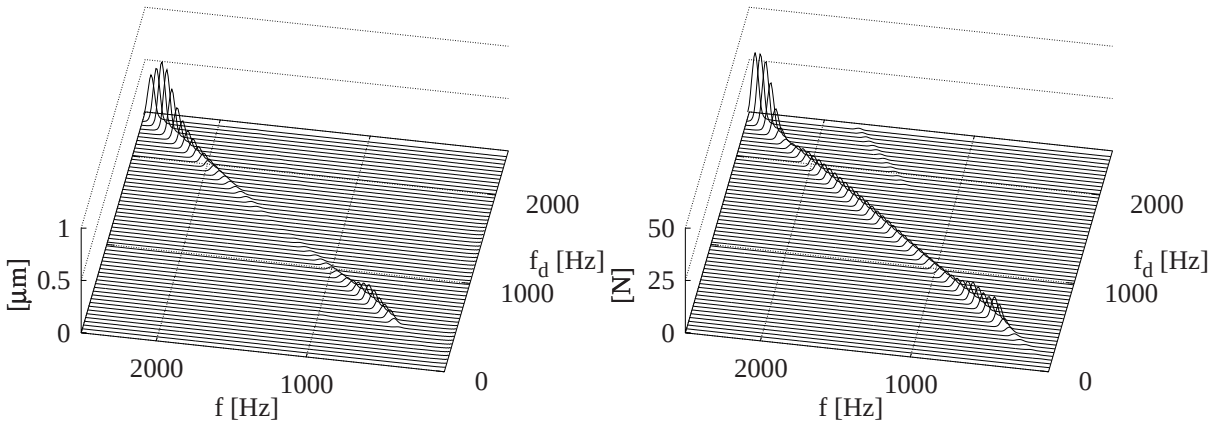

Figure 6: Support in roller bearings with squeeze film damper: displacement of the compressor wheel (left), bearing force(right) .

To increase the damping ratio of ball bearings it is common practice, for example in aeroplane engines, to add a squeeze film damper around the outer ring. A squeeze film damper is

a oil filled chamber which is similar to a fluid bearing. Distinctive is the pressure generation which is induced only by the radial movement of the ball bearing with respect to the pedestal without rotation. The production of this kind of support is much more costly but it combines the advantages of ball bearings including their high and constant stiffness with the damping ratio of fluid bearings. As Figure 6 illustrates the behaviour is similar to Figure 5 but the vibration level during the first and second resonance is reduced and the bearing forces are lowered significantly.

4 CONCLUSIONS

A fully nonlinear model of a turbocharger and the support of the elastic shaft was presented. The modelling depth of the analysed bearing variants is physically motivated and allows to transfer the methods without any loss of generality to other models with differing dimensions. Although the effort to solve the nonlinear equations of motion with strongly nonlinear forces is much higher than the solution of linear systems for example with linearised force laws, a dynamical run-up simulation of the entire system was performed economically justifiable.
The results were examined and benchmarked concerning unbalance response, subsynchronous frequencies and bearing forces. The presented algorithms can also be used in other applications and are not restricted to turbochargers in general.

REFERENCES

[1] T. Yamamoto and Y. Ishida, *Linear and Nonlinear Rotordynamics. A Modern Treatment with Applications.*, John Wiley & Sons Inc, New-York, 2001

[2] A. Muszynska, *whirl and whip-rotor/bearing stability problems*, Journal of Sound and Vibration Vol. 110, 1986

[3] F. Pfeiffer, *Einführung in die Dynamik*, B. G. Teubner, Stuttgart, 1992

[4] H. Hertz, *Über die Berührung fester elastischer Körper*, Journal für die reine und angewandte Mathematik, 1881.

[5] E. Woschke, C. Daniel, S. Nitzschke and J. Strackeljan: *Numerical run-up simulation of a turbocharger with full floating ring bearings*, In: The 10th International Conference on Vibration Problems, 2011.

[6] S. Nitzschke, E. Woschke, C. Daniel and J. Strackeljan, *Simulation von Schwimmbuchsenlagerungen in Abgasturboladern*, Journal of Mechanical Engineering of the National Technical University of Ukraine KPI, 2011

[7] C. Daniel, S. Nitzschke, E. Woschke and J. Strackeljan, *Numerische Simulation des instationären Verhaltens der Schwimmbuchsenlagerung in Turboladern*, 9. Internationale Tagung Schwingungen in rotierenden Maschinen, 2011

[8] B. Schweizer, *Vibrations and bifurcations of turbocharger rotors*, International Conference on Vibrations in Rotating Machines, Austria, 2009